pH and Ultrasound Dual-responsive Drug Delivery System Based On PEG–folate-functionalized Iron-based Metal–Organic Frameworks for Targeted Doxorubicin Delivery

Ahmed Ahmed[1], Abdollah Karami[1], Rana Sabouni[1*], Ghaleb A. Husseini[1], Vinod Paul[1]

[1] Department of Chemical Engineering, American University of Sharjah, Sharjah 26666, UAE

* Corresponding author: Rana Sabouni (rsabouni@aus.edu), American University of Sharjah, Sharjah 26666, United Arab Emirates

Abstract

In recent years, the use of metal–organic frameworks (MOFs) as drug nanocarriers has gained attention because of their extraordinary physical and chemical properties. In this work, dual-responsive iron-based MOFs were synthesized via the microwave-assisted method using $FeCl_3.6$ (H_2O) as the metal cluster and 2-aminoterephthalic acid (NH_2-BDC) as the organic linker (namely NH_2-Fe-BDC) and loaded with the anti-cancer drug doxorubicin (DOX). The DOX-loaded MOFs were further functionalized with polyethylene glycol-folate (PEG–FA), yielding PEG–FA-NH_2-Fe-BDC. The folate moiety is used to specifically target several cancers overexpressing the folate receptor (FR). These nanoparticles were characterized using Fourier-Transform Infrared Spectroscopy (FTIR), X-ray Diffraction (XRD), Thermogravimetric Analysis (TGA), and Dynamic Light Scattering (DLS). The FTIR confirmed the PEG–FA conjugation to the MOFs, while the XRD patterns confirmed the crystallinity of the

https://doi.org/10.1016/j.colsurfa.2021.127062

nanoparticles. TGA results demonstrated the thermal stability of the MOFs. Moreover, the DLS analysis showed that regular MOFs had a particle diameter of 577 nm, while the PEG–FA-functionalized MOF had a particle diameter of 461 nm, which demonstrates the improved colloidal stability of the functionalized MOF. The DOX encapsulation efficiency was determined to be approximately 97%, while the encapsulation capacity was around 14.5 wt.%. Furthermore, the *in-vitro* release profiles were studied under different pH values (5.3 and 7.4) with and without low-frequency ultrasound (LFUS, at 40 kHz). The results confirmed the sonosensitivity of the nanovehicles, with US-triggered release efficiency reaching up to 90% after 280 min (at a pH of 5.3). The MTT study revealed that these nanocarriers are non-toxic at lower concentrations. Their toxicity increases at higher concentrations. Furthermore, the cellular uptake was investigated via flow cytometry, and the results showed that conjugation of PEG-FA moiety to the MOF's surface significantly enhanced the targeting uptake of cancer cells. Accordingly, this study showed the pH/US dual-responsive capability of NH_2-Fe-BDC and PEG–FA-NH_2-Fe-BDC.

Keywords: metal–organic frameworks; drug delivery; ultrasound; triggered release; encapsulation efficiency; Doxorubicin, NH_2-Fe-BDC

1. INTRODUCTION

Cancer is a persistent public health problem around the world. According to epidemiological studies, cancer-related mortalities are expected to reach 13.1 million by 2030 [1]. Among cancer treatment methods, chemotherapy remains the most widely used [2]. However, chemotherapeutic agents do not affect cancerous or malignant cells only, but rather many other healthy cells in the body, causing many debilitating side effects that adversely affect the quality of life of the patient [3]. In addition, direct administration of anti-cancer drugs is often hindered by the drug's limited solubility,

poor physiological stability, and bioavailability [4]. As such, drug delivery systems (DDSs) can overcome some of these limitations. Recent advancements have shown that drug carriers can be used as an effective method to protect, increase the drug's bioavailability, and prolong its presence in the blood [5]. Additionally, the release of the encapsulated drug can be designed and controlled according to the type of material used to synthesize the DDS. Several organic and inorganic nanocarriers have been investigated as DDSs, including liposomes, micelles, quantum dots, mesoporous silica, carbon nanotubes, zeolites, and metal-organic frameworks [6–11].

Metal-organic frameworks (MOFs) are porous hybrid materials typically formed by the self-assembly of inorganic nodes like metal ions or clusters and organic linkers. Recently, nano-scaled MOFs have gained considerable attention in biomedical applications due to their unique physical and chemical properties, including a huge internal surface area that exceeds 6000 m^2/g and high porosity that reaches up to 90% of its volume [12,13]. The large surface area and pore volume enable high drug encapsulation efficiency making MOFs attractive as DDSs compared to other nanocarriers. An additional important characteristic of MOFs is the ease of structural tuning and surface modification, which gives scientists the capability to design MOF-based DDSs with dual therapeutic and diagnostic functionalities [14,15].

Recently, the field of drug delivery has witnessed exciting developments with the advent of stimuli-responsive MOF-based DDSs. These nanoplatforms are responsive to external or internal stimuli by undergoing a structural change that enables drug release from their cores. Stimuli-responsive DDSs offer the possibility of drug delivery in a temporal, targeted, and dosage-controlled manner, which enhances the drug delivery efficacy, while minimizing the side-effects [11,16]. Internal stimuli, which are related to the tumor microenvironment (TME), include pH, redox, ATP, and ions, while

external stimuli include light, heat, electrical waves, magnetic field, ultrasound, and microwaves [9–11,16]. There is growing interest in the development of multistimuli-responsive MOFs as the next-generation DDSs. Such nanoplatforms can utilize two or more, often a combination of internal and external, stimuli to trigger controlled and targeted drug release. One of the most reported combinations is the pH/near-infrared (NIR)-responsive DDSs. Such DDSs combine the controlled anti-cancer drug delivery with the therapeutic effects achieved by the DDS's light-responsive functionality, namely, photodynamic therapy (PDT) and photothermal therapy (PTT) [17–19].

A less-investigated example of dual-responsive MOF-based DDSs is pH/ultrasound-responsive DDSs [20]. Ultrasound (US) is currently investigated as a promising release-triggering stimulus in the drug delivery field [21–26]. The noninvasive US application can enhance the nanocarriers' transport into targeted cells due to thermal effects and mechanical stresses [11,22,27,28]. Furthermore, the oscillatory formation of US-induced microbubbles in biological tissues causes stresses on the nanocarrier's structure resulting in the enhanced release of the encapsulated drug [21,23,29].

Herein, we report a pH/US dual-responsive MOF-based drug delivery system (DDS) based on iron (Fe) as the metal cluster and 2-amino-1,4-benzenedicarboxylic acid (NH_2-BDC) as the organic linker. These MOFs are then functionalized with polyethylene glycol and folate (PEG–FA) to enhance the colloidal stability and targeting capability of the MOF-based DDS, since many cancerous tumors express high folate-receptor levels on their surface [30]. The synthesized MOFs were characterized using X-ray diffraction (XRD), Fourier-transform infrared (FTIR) analysis, thermogravimetric analysis (TGA), and dynamic light scattering (DLS). In addition, to demonstrate the pH/US dual-responsive capability of the DDS, the chemotherapeutic

drug doxorubicin (DOX) was loaded into the MOF, and the *in-vitro* drug release profiles were measured in phosphate-buffered saline (PBS) at two pH levels (namely, 7.4 and 5.3) and 37 °C with and without US. Moreover, the biocompatibility and cytotoxicity of the functionalized MOF were investigated using the MTT assay. Several concentrations of our newly synthesized MOFs were incubated with MCF-7 breast cancer cells.

2. EXPERIMENTS

2.1. Materials

All the chemicals and reagents used in the MOFs' synthesis and functionalization were purchased from Sigma-Aldrich (supplied through LABCO LLC. Dubai, United Arab Emirates) and used without further modifications. Iron (III) chloride hexahydrate ($FeCl_3.6H_2O$), 2-aminoterephthalic acid (NH_2-BDC) and N,N-dimethylformamide (DMF, ReagentPlus®, ≥ 99%) were used in the synthesis of NH_2-Fe-BDC. Furthermore, Folate-PEG2000-COOH (PEG–FA), N-(3-dimethylaminopropyl)-N'-ethylcarbodiimide hydrochloride (EDC), and N-hydroxysuccinimide (NHS) were used in the surface modification and PEG functionalization of the MOF. Doxorubicin (DOX) was obtained from Euroasia Trans Continental (Mumbai, India).

2.2. Synthesis of NH_2-Fe-BDC

The amino-functionalized MOF (NH_2-Fe-BDC) was synthesized using the microwave-assisted technique. First, 54 mg of $FeCl_3.6(H_2O)$ and 36 mg of NH_2-BDC were dissolved in 10 ml DMF. The solution was placed in a microwave reaction vessel and heated via microwave irradiation (SINEO, model MDS-6G, Shanghai, China) at 800 W and 135 °C for 99 minutes. Next, the resultant particles were separated by centrifugation at 4500 rpm for 15 minutes (Heraeus Megafuge 8R, Thermo Scientific, Waltham, MA, USA). Then, the resulting particles were washed with DMF and

centrifuged twice to remove unreacted precursors. The collected particles, namely NH_2-Fe-BDC MOF, were dried overnight in an oven at 100 ˚C.

2.3. DOX encapsulation in NH_2-Fe-BDC

To encapsulate DOX into the MOFs, 15 mg of NH_2-Fe BDC MOF were added to a 1-mM DOX dissolved in a PBS solution (pH of 7.4) and mixed for 24 hours. The mixture was then centrifuged at 4500 rpm for 30 minutes, the supernatant was removed and analyzed using UV-Vis spectroscopy (Evolution 60S, Thermo Scientific, Waltham, MA, USA). The DOX-loaded MOFs were then washed twice, centrifuged, and dried in an oven at 100 ˚C for 1 hour. After drying, the drug-loaded MOFs were stored in a desiccator for further surface modification. To calculate the drug loading efficiency, the following equation was used:

$$Loading\ efficiency\ (\%) = \frac{A_i - A_f}{A_i} \times 100 \quad (1)$$

where A_i and A_f are the absorbance values of the initial and final DOX concentrations. The characteristic peak of DOX was 480 nm.

Additionally, the loading capacity of the drug is calculated using the following equation:

$$Loading\ capacity\ (wt.\%) = \frac{m_{loaded}}{m_{loaded} + m_{MOF}} \times 100 \quad (2)$$

where m_{loaded} is the mass of DOX (mg) and m_{MOF} is the mass of the MOF before loading (mg).

2.4. PEG-Folate functionalization

In this study, the surface of the synthesized NH_2-Fe-BDC MOF was modified through post-synthesis modification steps to enhance targeting. The synthesized MOF underwent surface functionalization by conjugating a PEG functional group and folic acid, resulting in PEG–folate-functionalized MOF samples (PEG–FA-NH_2-Fe-BDC).

The folate functionalization of the NH_2-Fe-BDC MOFs was carried out as follows: 15 mg of the DOX-loaded NH_2-Fe-BDC was added to 10 ml PBS solution (pH 7.4) containing PEG–FA (0.75 mg), EDC (15 mg), and NHS (30 mg). Next, the mixture was incubated at room temperature for 3 hours. Finally, the samples were centrifuged, dried in an oven at 80 ºC, and stored in a desiccator at room temperature for further use.

2.5. Characterization

The MOF samples were characterized using several characterization tests, including X-ray diffraction (XRD), Fourier-transform infrared (FTIR) spectroscopy, thermogravimetric analysis (TGA), and dynamic light scattering (DLS). The XRD patterns were obtained using a Bruker D8 Advance X-ray diffractometer (Billerica, Massachusetts, USA) at room temperature using a Cu Kα radiation source (λ = 1.54 Å) on a silicon wafer from 5.0 to 50º (2θ) with a step size of 0.02º and 1s (per step) in a continuous mode. The FTIR spectra were measured on an FTIR instrument (PerkinElmer, Waltham, Massachusetts, USA) using the KBr pellet transmission technique, operating in the range of 4000 to 450 cm^{-1}, with a step of 1.0 cm^{-1}. For each sample, the spectrum was measured ten times and the average was reported. The TGA tests were performed using a Pyris 1 TGA instrument (PerkinElmer, USA) at a heating rate of 10 °C.min^{-1} from 30 °C to 800 °C. The particle size distribution, average particle diameter, and polydispersity index (PDI) of the samples were determined using a dynamic light scattering instrument (DynaPro NanoStar, Wyatt Technology, Santa Barbara, CA, USA). The results were averaged over 10 acquisitions. Scanning electron microscopy (SEM) was used to investigate the MOFs' surface morphology and shape (TESCAN VEGA3, Brno, Czech Republic).

2.6. DOX *in-vitro* release

In-vitro drug release experiments were conducted as follows: 15 mg of DOX-loaded MOFs (NH_2-Fe-BDC@DOX and PEG–FA-NH_2-Fe-BDC@DOX) were added to 0.01 M PBS solution at two different pH levels (i.e., 7.4 and 5.3) at a temperature of 37 °C. Then, low-frequency 40-kHz ultrasound at a power density of ~ 1 W/cm^2 was applied to the samples (10 min cycle) in a sonication bath (SHE-UT8031-EUK, Shesto, Watford, UK). After each sonication cycle, the samples were centrifuged, and an aliquot (3 ml) was taken from the supernatant for UV-Vis spectroscopic analysis. The same amount of the aliquot was replaced with fresh PBS for the next release cycle. The release procedure was repeated until maximum release was reached. Control *in-vitro* release experiments were also conducted without ultrasound. All experiments were performed in triplicates, and the average release profiles were reported. To calculate the cumulative release efficiency, the following equation is used:

$$Cumulative\ release\ efficiency\ (\%) = \sum_i \left(\frac{C_i}{C_m}\right) \quad (3)$$

where C_i is the DOX aliquot concentration at each time point and C_m is the DOX maximum release concentration determined using the spectroscopic analysis of the supernatant collected from the loading step.

2.7. *In-vitro* cytotoxicity analysis

The cytotoxicity of NH_2-Fe-BDC and PEG–FA-NH_2-Fe-BDC was assessed by the MTT assay. For the assay, MCF-7 breast cancer cells, maintained in RPMI-1640 media, were seeded in 24-well plates at a density of 5 x10^4 cells per well. After overnight incubation at 37 °C and 5% CO_2, the media was replaced with fresh media containing the nanoparticles at different concentrations (i.e., 15.625, 31.25, 62.5, 125, 250, 500 and 1000 µg/ml). All experiments were performed in triplicates. Before adding to the wells, the media containing the nanoparticles were sonicated in an ultrasonic bath to ensure the nanoparticles' well-dispersion. The treated cells were then further

incubated for 48 hours; the wells with no treatment were used as the control. Subsequently, the media in the wells were replaced with new media containing 0.5 mg/ml MTT reagent and incubated for 4 h to allow the formation of formazan crystals. These formazan crystals were then fully dissolved by removing the MTT-medium mixture from the wells and adding 250 µl DMSO. The solutions were then transferred to 96-well plates and the absorbance (of the resultant purple color) was measured by a microplate reader at 600 nm (Metertech M965 microplate reader, Taiwan). The cell viability was calculated as follows:

$$\%Cell\ viability = \frac{\text{Average absorbance value of treatment group}}{\text{Average absorbance value of control}} \times 100 \quad (4)$$

The cytotoxicity experiments were run in triplicates.

2.8. Cellular internalization (uptake)

MCF-7 cell lines were trypsinized and seeded into 6-well plates at a concentration of 6 x 10^5 cells per well. After 24 hours of incubation at 37 °C and 5% CO_2, the media in the wells were changed with fresh media containing DOX-loaded NH_2-Fe-BDC and PEG-FA-NH_2-Fe-BDC for cellular internalization studies. The final concentration of MOF was 20 µg/ml of media; the cells were then incubated for 3 more hours. Following the incubation, the cells were then washed with PBS and collected in 15-ml falcon tubes after trypsinization and washed twice by centrifugation with PBS. The cells (10,000 events) were then analyzed in a flow cytometer (Beckman Coulter FC 500, Brea, CA, USA). The experiments were performed in triplicates and the mean fluorescence was reported for each treatment.

3. RESULTS AND DISCUSSION

3.1. Characterization

The XRD patterns of the samples are shown in Figure 1. The patterns are

comparative with previously reported results [31–33]. The characteristic peaks are detected in the low 2θ range (5–20°), specifically, 2θ = 9, 10, 13, 16 and 20°. Furthermore, the XRD patterns of the DOX-loaded PEG–FA-functionalized MOF exhibited lowered intensity and minor broadening of the signature peaks compared to the non-functionalized MOF, indicating a smaller crystal size as well as the encapsulation of DOX molecules without co-crystallization into the MOF nanoparticles [34]. The successful DOX loading and PEG–FA functionalization were also confirmed by the change in the particles' color, as shown in the insets of Figure 1. A schematic representation of the PEG-FA moiety's attachment to the crystal structure as well as DOX encapsulation in the nanoparticle's pores is presented in Figure 2.

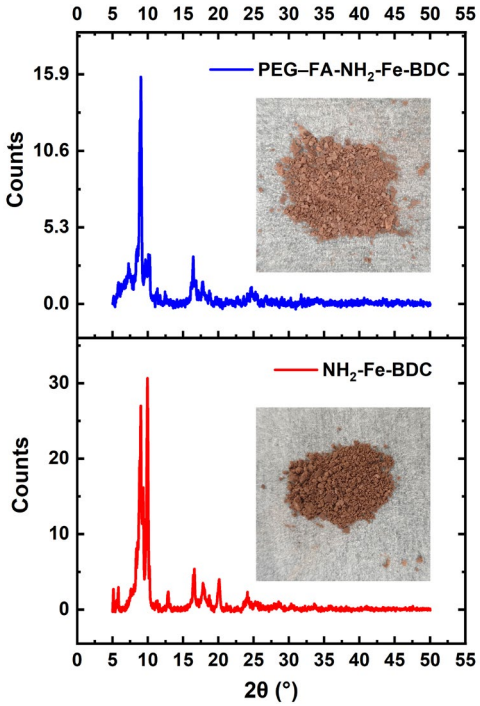

Figure 1: XRD patterns of NH_2-Fe-BDC and DOX-loaded PEG–FA-NH_2-Fe-BDC. The insets represent the pictures of the synthesized samples.

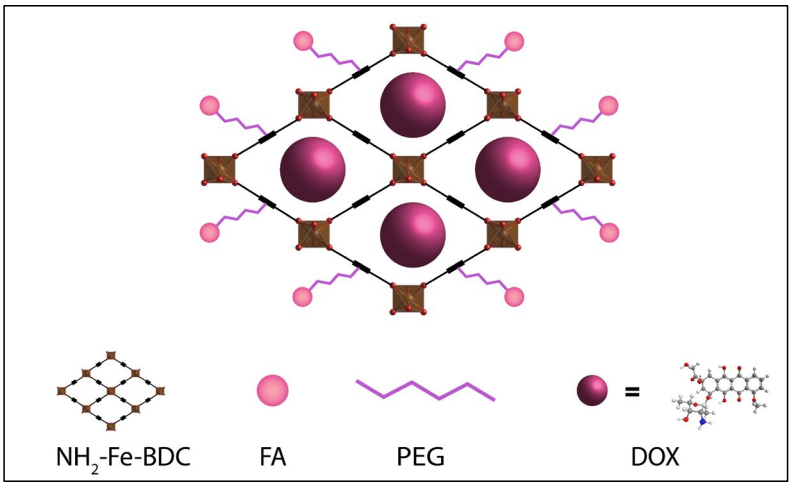

Figure 2: Schematic representation of DOX encapsulation and PEG–FA attachment

The measured FTIR spectra of the synthesized MOFs in Figure 3 show the characteristic transmittance bands of the NH_2-Fe-BDC and PEG–FA-NH_2-Fe-BDC MOFs. The presence of the double peaks in the NH_2-Fe-BDC IR spectrum at around 3465 and 3370 cm^{-1} can be assigned to the symmetric/asymmetric stretching of the NH_2 group [5,35,36]. The presence of the carboxylate group of the organic linker can be inferred from the symmetric and asymmetric vibration peaks at around 1380 and 1579 cm^{-1}, respectively [35]. Furthermore, the peak at around 1254 cm^{-1} corresponds to the bond stretching of the aromatic carbon and nitrogen (C–N), while the peak at around 769 cm^{-1} is attributed to the Fe–OH bond in the metal cluster unit of the crystal [36]. For the PEG–FA-NH_2-Fe-BDC sample, the IR spectrum show peaks at around 1054, 2910, and 3435 cm^{-1} signaling a successful attachment of the PEG–FA group [37].

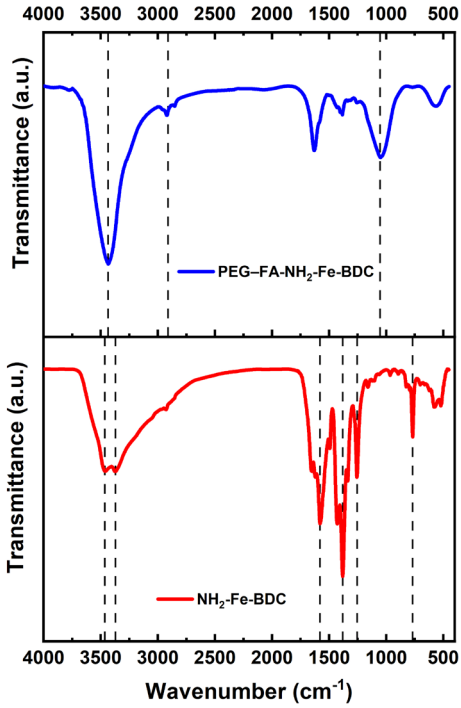

Figure 3: FTIR spectra of NH_2-Fe-BDC and PEG–FA-NH_2-Fe-BDC

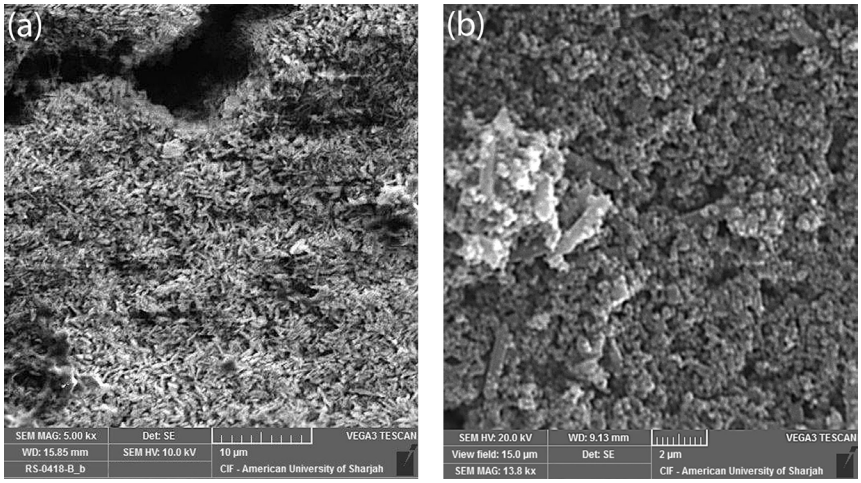

Figure 4: SEM images of a) NH_2-Fe-BDC and b) Dox-loaded PEG–FA-NH_2-Fe-BDC samples

The SEM images in Figure 4 show a narrow needle-shaped crystal for NH_2-Fe-BDC nanoparticles (Figure 3a), which is mainly attributed to the NH_2-BDC ligand in the framework [38]. The DOX-loaded PEG–FA-NH_2-Fe-NH2-BDC nanoparticles, on the other hand, have more rounded-shaped crystals with less-defined edges (Figure 3b), which may be attributed to the PEG–FA conjugation and DOX encapsulation into the nanoparticles [39].

To analyze the thermal stability of the synthesized MOFs, thermogravimetric analysis (TGA) was performed. Figure 5 represents the percentage weight loss (wt.%) profile and its derivative as a function of temperature. The first reduction in weight (20% wt. loss%) in the range 30–300 °C corresponds to the removal of water and DMF confined within the MOF's pores, while the more pronounced wt.% that appears in the temperature range 300–700 °C is due to the decomposition of the MOF's framework. The TGA results demonstrate the good thermal stability of the synthesized MOFs.

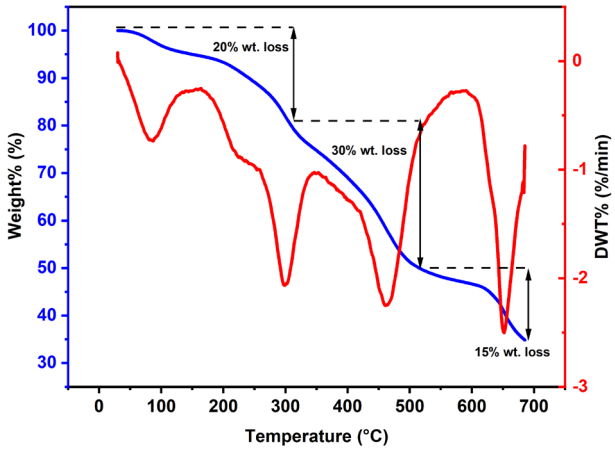

Figure 5: Thermogravimetric analysis (TGA) profile of NH_2-Fe-BDC

The particle size distribution of NH_2-Fe-BDC and PEG–FA-NH_2-Fe-BDC was determined using the DLS measurement of samples dispersed in PBS solutions (pH 7.4,

around 24 µg/ml) and based on a spherical particle-shape assumption. The results are presented in Figure 6 and show that NH_2-Fe-BDC nanoparticles have an average hydrodynamic diameter of 577 nm, while the PEG–FA-NH_2-Fe-BDC have an average hydrodynamic diameter of 461 nm, which are suitable particle diameters for *in vitro* and *in vivo* applications [40,41]. These results indicate that PEG-FA functionalization enhanced the nanoparticles' dispersion in the solution, reducing their aggregation and increasing their colloidal stability [39].

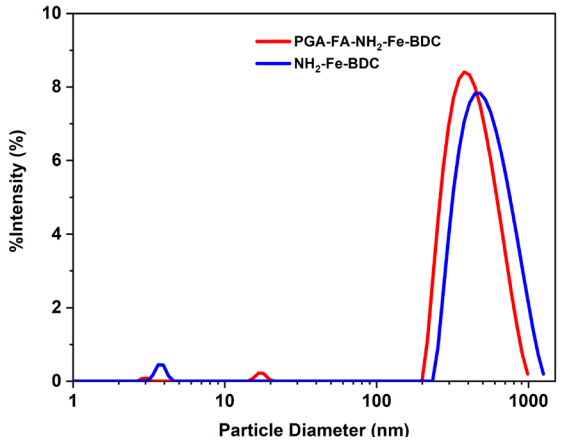

Figure 6: Particle size distribution of NH_2-Fe-BDC and PEG–FA-NH_2-Fe-BDC

3.2. DOX encapsulation and *In-vitro* release profiles

The DOX concentration in PBS was calculated based on the calibration curve presented in Figure 7. Then, the loading efficiency and capacity of the MOF samples were determined by measuring the UV-Vis absorbance spectra of the loading supernatant after centrifugation and the values were calculated based on equations (1) and (2). The average DOX loading efficiency and capacity for DOX@NH_2-Fe-BDC were found to be ~ 97.4% and 14.5 wt.%, respectively, while the DOX@PEG-FA-NH_2-Fe-BDC nanoparticles had an average loading efficiency and capacity of ~ 97.7% and 14.5 wt.%, respectively.

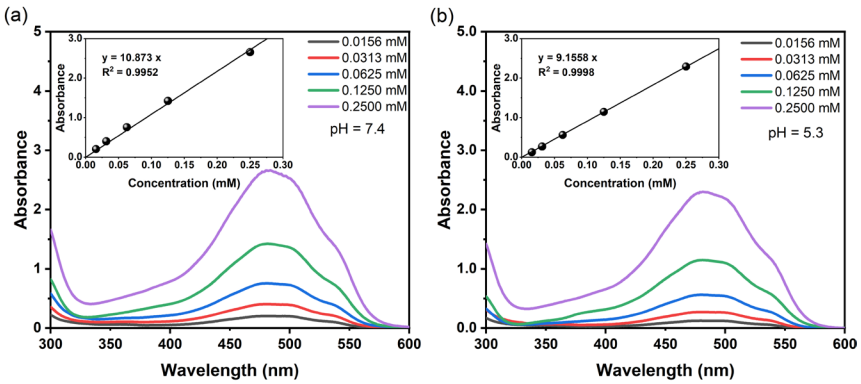

Figure 7: Absorbance spectra of standard DOX solutions in PBS (pH 5.3 and 7.4). Inset is the calibration curve

The *in-vitro* release experiments were conducted at two different pH conditions, 7.4 and 5.3, for DOX@NH_2-Fe-BDC and DOX@PEG–FA-NH_2-Fe-BDC MOFs. To investigate the sonosensitivity of the nanocarriers, release profiles of both DOX-loaded MOFs (DOX@NH_2-Fe-BDC and DOX@PEG–FA-NH_2-Fe-BDC) were reported with and without US at both pH values mentioned above. All experiments were conducted in triplicates and the average release and standard deviation were calculated and reported accordingly. The cumulative release profiles at pH 5.3 and 7.4 for the functionalized and non-functionalized nanocarriers are presented in Figure 8 (a-d). The results prove the pH/US dual responsive capability of both DOX@NH_2-Fe-BDC and DOX@PEG–FA-NH_2-Fe-BDC. The maximum US-triggered DOX release from NH_2-Fe BDC at pH 7.4 was around 44.4% in 280 min, compared to 90.9% at pH 5.3 (Figure 8(a-b)). Similarly, the maximum US-triggered release from the functionalized MOF increased from 36% (pH 7.4) to around 70.2% (pH 5.3) in the same time period (Figure 8(c-d)). These results demonstrate that the release is more effective at low pH values, which is preferable since the cancerous or tumor environment is more acidic compared to the healthy tissue, mainly due to anaerobic respiration and lactic acid build-up [20].

Moreover, by comparing the release from the DOX@NH_2-Fe-BDC to that from the DOX@PEG–FA-NH_2-Fe-BDC nanoparticles at the same pH, it was noticed that the functionalized MOFs had a lower *in-vitro* release percentage than the non-functionalized MOF. This decrease in release may be attributed to the fact that MOF loading/release efficiency depends on their surface morphology. Functionalization modifies the surface of the MOF and may, as a result, lower the drug's ability to be released from the pores of the MOF. Table 1 presents a comparison between various iron-based MOF nanocarriers based on their encapsulation, release, cytotoxicity, and targeting functionality.

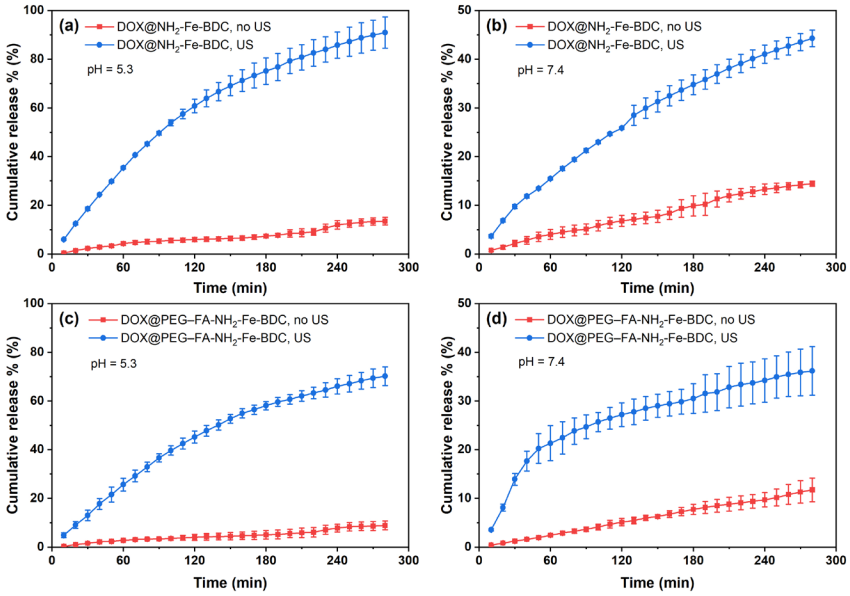

Figure 8: *In-vitro* DOX release profiles. The error bars represent the standard deviation of the three replicates, while the points represent the average of these three independent replicates

Table 1: Summary of the loading capacities, release efficiencies, cytotoxicity, and targeting-functionality of various iron-based MOF nanocarriers

MOF nanocarrier	Stimulus	Loading capacity (wt.%)	Release rate (%)	Cytotoxicity	Targeting functionality	Reference
Fe-NDC	US	13.37	80% (245 min, PBS, pH 7.4)	Cytotoxicity against MCF-7 cells showed good biocompatibility (95.95-85.11% cell viability at 12.5-200 µg/ml Fe-NDC concentration). Half-maximal inhibitory concentration (IC_{50}) towards MCF-7 cells was 1022 µg/ml.	–	[26]
MIL-100(Fe)	–	9.1	100% (13 days, PBS, pH 7.4)	–	–	[42]
Fe-BTC	–	6.5	69% (16 days, PBS, pH 7.4)	–	–	[43]
MN@Fe-BTC	–	2.2	21% (16 days, PBS, pH 7.4)	–	Magnetic field-targeted drug delivery	
MIL-100(Fe) (DM NPs)	pH	11 – 32.5 (with different MOF/DOX weight ratio)	66% (60 h, PBS, pH 5.5) 30% (60 h, PBS, pH 7.4)	MCF-7 cells co-incubated with MIL-100 at different concentrations retained high cell viability of about 90% up to 200 µg/ml MIL-100 concentration. DMH NPs exhibited stronger cytotoxicity than DM NPs toward MCF-7 cells within the experimental concentration range (DOX concentration 0.1 to 10 µg/ml).	–	[44]
HA-MIL-100(Fe) (DMH NPs)	pH	11 – 32.5 (with different MOF/DOX weight ratio)	~50% (60 h, PBS, pH 5.5) ~25% (60 h, PBS, pH 7.4)		Hyaluronic acid (HA)-mediated targeting specificity	
$NaGdF_4$:Yb/Er@ MIL-53(Fe)/FA	pH	16	80% (48 h, PBS, pH 5.2) 67.5% (48 h, PBS, pH 7.4)	Cytotoxicity was tested against B16−F10 cells. For $NaGdF_4$:Yb/Er@MIL-53(Fe)/FA, >80% cell viability was observed up to 5 µg/ml concentration. For the DOX-loaded NPs, cell viability was <40% at 5 µg/ml concentration.	Folate receptor targeting specifity	[45]
NH_2-Fe-BDC	pH and US	14.5	44.4% (280 min, PBS, pH 7.4, US) 90.9% (280 min, PBS, pH 5.3, US)	Cytotoxicity in MCF-7 cells showed excellent biocompatibility. The cell viability was >65% up to 1000 µg/ml NPs concentration	–	This work
PEG-FA-NH_2-Fe-BDC	pH and US	14.5	36% (280 min, PBS, pH 7.4, US) 70.2% (280 min, PBS, pH 5.3, US)	Cytotoxicity in MCF-7 cells via MTT assay showed 38% cell viability up to 1000 µg/ml NPs concentration	Folate receptor targeting specifity	

Commented [GH1]: Please use the table in the rebuttal. I made some changes there.

3.3. *In-vitro* cytotoxicity analysis

The cytotoxicity was investigated by treating the MCF-7 cell lines with the MOF nanoparticles at different concentrations. The results are shown in Figure 9; PEG–FA-NH_2-Fe-BDCs were slightly more cytotoxic compared to NH_2-Fe-BDC. At low concentrations, the cell viability was high for NH_2-Fe-BDC, and as the concentration increased, the viability decreased.

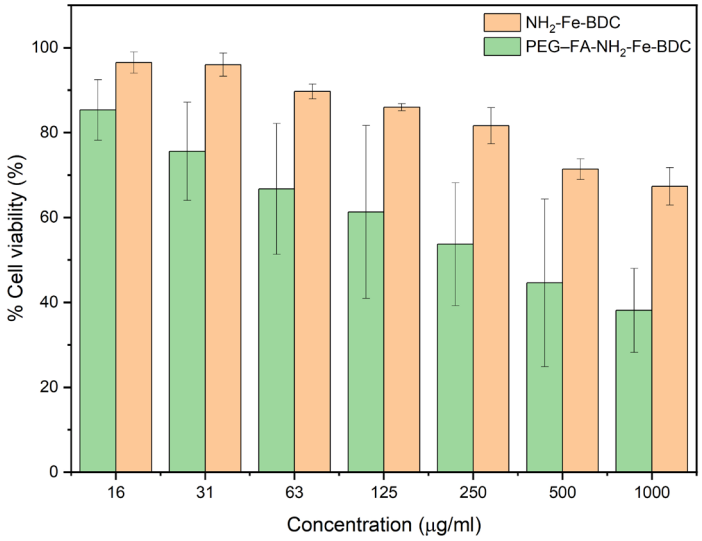

Figure 9: Cytotoxicity analysis of NH_2-Fe-BDC and PEG-FA-NH_2-Fe-BDC via MTT assay

3.4. Cellular internalization (uptake)

The well plates treated with DOX@PEG-FA-NH_2-Fe-BDC showed a higher mean fluorescent intensity compared to DOX@NH_2-Fe-BDC which relates to a higher uptake of the MOF nanoparticles by the cell line. The enhanced uptake was due to overexpressed folate receptors on MCF-7 cell line, binding to the folate moiety attached to the MOF, the nanoparticles were then taken up by the cells by receptor mediated endocytosis. On average the cellular internalization measured by the mean

fluorescent intensity of cells treated with DOX@PEG-FA-NH_2-Fe-BDC were 125% (± 37%) higher compared to DOX@NH_2-Fe-BDC (n=3). The avergae fluorescent intensity of the different cellular populations treated with DOX@NH_2-Fe-BDC and DOX@PEG-FA-NH_2-Fe-BDC is presented in Figure 10.

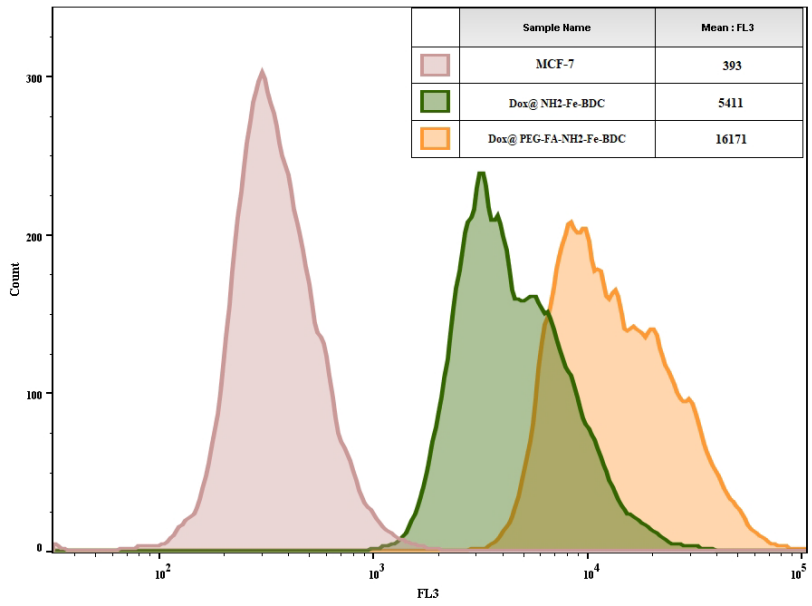

Figure 10: The flow cytometry analysis of the cellular uptake of the DOX-loaded nanoparticles (Flourescense is the average of three experiments)

Commented [GH2]: Please use the section in the rebuttal.

4. CONCLUSION

In conclusion, an iron-based NH_2-Fe BDC MOF was successfully synthesized using microwave-assisted synthesis. In addition, PEG–FA was conjugated to the surface of the MOF, using a post-synthesis modification technique as a cancer biomarker targeting ligand. Characterization tests were performed, including FTIR, TGA, and DLS to analyze the morphology, thermal stability, and particle size distribution of the MOF samples. The results of the characterization tests showed the successful synthesis and the successful PEG–FA attachment, in addition to the excellent

thermal stability and a suitable particle diameter for *in vitro* and *in vivo* applications. The chemotherapeutic drug DOX was successfully loaded in the MOF. The MOF achieved an appropriate DOX loading efficiency of ~ 97% and 14.5 wt.% loading capacity. The use of ultrasound was utilized as an external release stimulus. The *in-vitro* release profiles in PBS were obtained at pH levels of 5.3 and 7.4 at 37 $^{\circ}$C. The cumulative DOX release efficiencies with US were around 44.4 % and 90% at pH levels of 7.4 and 5.3, respectively. Moreover, the PEG–FA functionalization was investigated as a targeting mechanism for cancerous tissues in conditions mimicking the tumor microenvironment. The *in-vitro* cumulative DOX release of PEG–FA-NH_2-Fe-BDC was around 70.2% and 36 % at pH levels of 5.3 and 7.4, respectively. The MTT results confirmed the low toxicity of these nanocarriers at concentrations relevant to their use *in vivo* and future clinical trials, while flow cytometry indicated the higher drug internalization and hence performance of DOX@PEG-FA-NH_2-Fe-BDC compared to DOX@NH_2-Fe-BDC. This study showed the pH/US dual-responsive capability of NH_2-Fe-BDC and PEG–FA-NH_2-Fe-BDC.

Acknowledgment:

The work was supported by the American University of Sharjah via the faculty research grants [grant numbers: EFRG18-BBR-CEN-03, FRG20-M-E84, FRG20-L-E48]. The authors gratefully acknowledge the help of the Advanced Materials Research Lab at the University of Sharjah in conducting XRD and FTIR characterization tests.

Conflict of Interest

The authors declare no conflict of interest. The authors declare no competing financial interest.

REFERENCES

[1] Ö. Sönmez, Z. Yalçın, E. Karakeçe, İ. Çiftci, T. Erdem, Associations between Demodex species infestation and various types of cancer, Acta Parasitol. 58 (2013) 551–555. https://doi.org/10.2478/s11686-013-0178-y.

[2] V.T. DeVita, E. Chu, A History of Cancer Chemotherapy, Cancer Res. 68 (2008) 8643–8653. https://doi.org/10.1158/0008-5472.CAN-07-6611.

[3] A.E. Kayl, C.A. Meyers, Side-effects of chemotherapy and quality of life in ovarian and breast cancer patients, Curr. Opin. Obstet. Gynecol. 18 (2006) 24–28. https://doi.org/10.1097/01.gco.0000192996.20040.24.

[4] C. Mohanty, M. Das, S.K. Sahoo, Emerging role of nanocarriers to increase the solubility and bioavailability of curcumin, Expert Opin. Drug Deliv. 9 (2012) 1347–1364. https://doi.org/10.1517/17425247.2012.724676.

[5] J. Liu, L. Zhang, J. Lei, H. Shen, H. Ju, Multifunctional Metal–Organic Framework Nanoprobe for Cathepsin B-Activated Cancer Cell Imaging and Chemo-Photodynamic Therapy, ACS Appl. Mater. Interfaces. 9 (2017) 2150–2158. https://doi.org/10.1021/acsami.6b14446.

[6] M. Díaz, P. Vivas-Mejia, Nanoparticles as Drug Delivery Systems in Cancer Medicine: Emphasis on RNAi-Containing Nanoliposomes, Pharmaceuticals. 6 (2013) 1361–1380. https://doi.org/10.3390/ph6111361.

[7] Y. Chen, H. Chen, J. Shi, Inorganic nanoparticle-based drug codelivery nanosystems to overcome the multidrug resistance of cancer cells, Mol. Pharm. 11 (2014) 2495–2510.

[8] J.J. Lee, L.S. Yazan, C.A. Abdullah, A review on current nanomaterials and their drug conjugate for targeted breast cancer treatment, Int. J. Nanomedicine. 12 (2017) 2373– 2384.

[9] Y. Wang, J. Yan, N. Wen, H. Xiong, S. Cai, Q. He, Y. Hu, D. Peng, Z. Liu, Y. Liu, Metal-organic frameworks for stimuli-responsive drug delivery, Biomaterials. 230 (2020) 119619. https://doi.org/10.1016/j.biomaterials.2019.119619.

[10] C. Carrillo-Carrión, Nanoscale metal–organic frameworks as key players in the context of drug delivery: evolution toward theranostic platforms, Anal. Bioanal. Chem. 412 (2020) 37–54. https://doi.org/10.1007/s00216-019-02217-y.

[11] S. Mura, J. Nicolas, P. Couvreur, Stimuli-responsive nanocarriers for drug delivery, Nat. Mater. 12 (2013) 991–1003. https://doi.org/10.1038/nmat3776.

[12] H. Furukawa, K.E. Cordova, M. O'Keeffe, O.M. Yaghi, The Chemistry and Applications of Metal-Organic Frameworks, Science (80-.). 341 (2013) 1230444–1230444. http://www.sciencemag.org/cgi/doi/10.1126/science.1230444.

[13] O.K. Farha, I. Eryazici, N.C. Jeong, B.G. Hauser, C.E. Wilmer, A.A. Sarjeant, R.Q. Snurr, S.T. Nguyen, A.Ö. Yazaydın, J.T. Hupp, Metal-organic framework materials with ultrahigh surface areas: is the sky the limit?, J. Am. Chem. Soc. 134 (2012) 15016–21. https://doi.org/10.1021/ja3055639.

[14] J.-C. Yang, Y. Chen, Y.-H. Li, X.-B. Yin, Magnetic Resonance Imaging-Guided Multi-Drug Chemotherapy and Photothermal Synergistic Therapy with pH and NIR-Stimulation Release, ACS Appl. Mater. Interfaces. 9 (2017) 22278–22288. https://doi.org/10.1021/acsami.7b06105.

[15] W. Liu, Y.-M. Wang, Y.-H. Li, S.-J. Cai, X.-B. Yin, X.-W. He, Y.-K. Zhang, Fluorescent Imaging-Guided Chemotherapy-and-Photodynamic Dual Therapy with Nanoscale Porphyrin Metal-Organic Framework, Small. 13 (2017) 1603459. https://doi.org/10.1002/smll.201603459.

[16] A. Jhaveri, P. Deshpande, V. Torchilin, Stimuli-sensitive nanopreparations for combination cancer therapy, J. Control. Release. 190 (2014) 352–370. https://doi.org/10.1016/j.jconrel.2014.05.002.

[17] J. Yao, J. Feng, J. Chen, External-stimuli responsive systems for cancer theranostic, Asian J. Pharm. Sci. 11 (2016) 585–595. https://doi.org/10.1016/j.ajps.2016.06.001.

[18] J.-Y. Zeng, M.-K. Zhang, M.-Y. Peng, D. Gong, X.-Z. Zhang, Porphyrinic Metal-Organic Frameworks Coated Gold Nanorods as a Versatile Nanoplatform for Combined Photodynamic/Photothermal/Chemotherapy of Tumor, Adv. Funct. Mater. 28 (2018) 1705451. https://doi.org/10.1002/adfm.201705451.

[19] S. Li, L. Zhang, X. Liang, T. Wang, X. Chen, C. Liu, L. Li, C. Wang, Tailored synthesis of hollow MOF/polydopamine Janus nanoparticles for synergistic multi-drug chemo-photothermal therapy, Chem. Eng. J. 378 (2019) 122175. https://doi.org/10.1016/j.cej.2019.122175.

[20] J. An, Y.-G. Hu, C. Li, X.-L. Hou, K. Cheng, B. Zhang, R.-Y. Zhang, D.-Y. Li, S.-J. Liu, B. Liu, D. Zhu, Y.-D. Zhao, A pH/Ultrasound dual-response biomimetic nanoplatform for nitric oxide gas-sonodynamic combined therapy and repeated ultrasound for relieving hypoxia, Biomaterials. 230 (2020) 119636. https://doi.org/10.1016/j.biomaterials.2019.119636.

[21] G.A. Husseini, W.G. Pitt, Micelles and Nanoparticles for Ultrasonic Drug and Gene Delivery, Adv. Drug Deliv. Rev. 60 (2008) 1137–1152.

[22] S. Ganta, H. Devalapally, A. Shahiwala, M. Amiji, A review of stimuli-responsive nanocarriers for drug and gene delivery, J. Control. Release. 126 (2008) 187–204.

[23] Q.-L. Zhou, Z.-Y. Chen, Y.-X. Wang, F. Yang, Y. Lin, Y.-Y. Liao, Ultrasound-

Mediated Local Drug and Gene Delivery Using Nanocarriers, Biomed Res. Int. 2014 (2014) 1–13. https://doi.org/10.1155/2014/963891.

[24] B. Mishra, B.B. Patel, S. Tiwari, Colloidal nanocarriers: a review on formulation technology, types and applications toward targeted drug delivery, Nanomedicine. 6 (2010) 9–24.

[25] G.A. Husseini, G.D. Myrup, W.G. Pitt, D.A. Christensen, N.Y. Rapoport, Factors affecting acoustically triggered release of drugs from polymeric micelles, J. Control. Release. 69 (2000) 43–52.

[26] M. Ibrahim, R. Sabouni, G.A. Husseini, A. Karami, R.G. Bai, D. Mukhopadhyay, Facile Ultrasound-Triggered Release of Calcein and Doxorubicin from Iron-Based Metal-Organic Frameworks, J. Biomed. Nanotechnol. 16 (2020) 1359–1369. https://doi.org/10.1166/jbn.2020.2972.

[27] I. Udroiu, Ultrasonic drug delivery in Oncology, JBUON. 20 (2015) 381–390.

[28] E.-K. Lim, E. Jang, K. Lee, S. Haam, Y.-M. Huh, Delivery of Cancer Therapeutics Using Nanotechnology, Pharmaceutics. 5 (2013) 294–317.

[29] K.G. Baker, V.J. Robertson, F.A. Duck, A Review of Therapeutic Ultrasound: Biophysical Effects, Phys. Ther. 81 (2001) 1351–1358. https://doi.org/10.1093/ptj/81.7.1351.

[30] B. Yang, M. Shen, J. Liu, F. Ren, Post-Synthetic Modification Nanoscale Metal-Organic Frameworks for Targeted Drug Delivery in Cancer Cells, Pharm. Res. 34 (2017) 2440–2450. https://doi.org/10.1007/s11095-017-2253-9.

[31] K.M.L. Taylor-Pashow, J. Della Rocca, Z. Xie, S. Tran, W. Lin, Postsynthetic Modifications of Iron-Carboxylate Nanoscale Metal−Organic Frameworks for Imaging and Drug Delivery, J. Am. Chem. Soc. 131 (2009) 14261–14263. https://doi.org/10.1021/ja906198y.

[32] X. Yin, B. Yang, B. Chen, M. He, B. Hu, Multifunctional Gold Nanocluster Decorated Metal–Organic Framework for Real-Time Monitoring of Targeted Drug Delivery and Quantitative Evaluation of Cellular Therapeutic Response, Anal. Chem. 91 (2019) 10596–10603. https://doi.org/10.1021/acs.analchem.9b01721.

[33] D. Wang, R. Huang, W. Liu, D. Sun, Z. Li, Fe-Based MOFs for Photocatalytic CO 2 Reduction: Role of Coordination Unsaturated Sites and Dual Excitation Pathways, ACS Catal. 4 (2014) 4254–4260. https://doi.org/10.1021/cs501169t.

[34] P. Markopoulou, N. Panagiotou, A. Li, R. Bueno-Perez, D. Madden, S. Buchanan, D. Fairen-Jimenez, P.G. Shiels, R.S. Forgan, Identifying Differing Intracellular Cargo Release Mechanisms by Monitoring In Vitro Drug Delivery from MOFs in Real Time, Cell Reports Phys. Sci. 1 (2020) 100254. https://doi.org/10.1016/j.xcrp.2020.100254.

[35] M. Almáši, V. Zeleňák, P. Palotai, E. Beňová, A. Zeleňáková, Metal-organic framework MIL-101(Fe)-NH 2 functionalized with different long-chain polyamines as drug delivery system, Inorg. Chem. Commun. 93 (2018) 115–120. https://doi.org/10.1016/j.inoche.2018.05.007.

[36] R. Liu, L. Chi, X. Wang, Y. Wang, Y. Sui, T. Xie, H. Arandiyan, Effective and selective adsorption of phosphate from aqueous solution via trivalent-metals-based amino-MIL-101 MOFs, Chem. Eng. J. 357 (2019) 159–168. https://doi.org/10.1016/j.cej.2018.09.122.

[37] Z. Shi, X. Chen, L. Zhang, S. Ding, X. Wang, Q. Lei, W. Fang, FA-PEG decorated MOF nanoparticles as a targeted drug delivery system for controlled release of an autophagy inhibitor, Biomater. Sci. 6 (2018) 2582–2590. https://doi.org/10.1039/C8BM00625C.

505 [38] M. Ma, A. Bétard, I. Weber, N.S. Al-Hokbany, R.A. Fischer, N. Metzler-Nolte,
506 Iron-Based Metal–Organic Frameworks MIL-88B and NH 2 -MIL-88B: High
507 Quality Microwave Synthesis and Solvent-Induced Lattice “Breathing,” Cryst.
508 Growth Des. 13 (2013) 2286–2291. https://doi.org/10.1021/cg301738p.
509 [39] I. Abánades Lázaro, S. Haddad, S. Sacca, C. Orellana-Tavra, D. Fairen-Jimenez,
510 R.S. Forgan, Selective Surface PEGylation of UiO-66 Nanoparticles for
511 Enhanced Stability, Cell Uptake, and pH-Responsive Drug Delivery, Chem. 2
512 (2017) 561–578. https://doi.org/10.1016/j.chempr.2017.02.005.
513 [40] S.K. Hobbs, W.L. Monsky, F. Yuan, W.G. Roberts, L. Griffith, V.P. Torchilin,
514 R.K. Jain, Regulation of transport pathways in tumor vessels: Role of tumor type
515 and microenvironment, Proc. Natl. Acad. Sci. 5 (1998) 4607–4612.
516 [41] J.X. Jiang, J.J. Keating, E.M.D. Jesus, R.P. Judy, B. Madajewski, O. Venegas,
517 O.T. Okusanya, S. Singhal, Optimization of the enhanced permeability and
518 retention effect for near-infrared imaging of solid tumors with indocyanine
519 green, Am. J. Nucl. Med. Mol. Imaging. 5 (2015) 390–400.
520 [42] P. Horcajada, T. Chalati, C. Serre, B. Gillet, C. Sebrie, T. Baati, J.F. Eubank, D.
521 Heurtaux, P. Clayette, C. Kreuz, J.-S. Chang, Y.K. Hwang, V. Marsaud, P.-N.
522 Bories, L. Cynober, S. Gil, G. Férey, P. Couvreur, R. Gref, Porous metal–
523 organic-framework nanoscale carriers as a potential platform for drug delivery
524 and imaging, Nat. Mater. 9 (2010) 172–178. https://doi.org/10.1038/nmat2608.
525 [43] M. Bellusci, P. Guglielmi, A. Masi, F. Padella, G. Singh, N. Yaacoub, D. Peddis,
526 D. Secci, Magnetic Metal–Organic Framework Composite by Fast and Facile
527 Mechanochemical Process, Inorg. Chem. 57 (2018) 1806–1814.
528 https://doi.org/10.1021/acs.inorgchem.7b02697.
529 [44] T. Xue, C. Xu, Y. Wang, Y. Wang, H. Tian, Y. Zhang, Doxorubicin-loaded

nanoscale metal–organic framework for tumor-targeting combined chemotherapy and chemodynamic therapy, Biomater. Sci. 7 (2019) 4615–4623. https://doi.org/10.1039/C9BM01044K.

[45] P. Mukherjee, A. Kumar, K. Bhamidipati, N. Puvvada, S.K. Sahu, Facile Strategy to Synthesize Magnetic Upconversion Nanoscale Metal–Organic Framework Composites for Theranostics Application, ACS Appl. Bio Mater. 3 (2020) 869–880. https://doi.org/10.1021/acsabm.9b00949.